ATLAS PUB Note

ATLAS-PHYS-PUB-2018-040

4th December 2018

Prospects for differential cross-section measurements of Higgs boson production measured in decays to ZZ and $\gamma\gamma$ with the ATLAS experiment at the High-Luminosity LHC

The ATLAS Collaboration

Prospects for Higgs boson differential cross section measurements for the full expected High-Luminosity LHC (HL-LHC) luminosity of 3 ab^{-1} are performed using the $H \to \gamma\gamma$, $H \to ZZ^* \to 4\ell$ decay channels, as well as their combination. Differential cross section measurements are presented for the Higgs boson transverse momentum, Higgs boson rapidity, number of jets produced together with the Higgs boson, and the transverse momentum of the leading jet.

ATL-PHYS-PUB-2018-040
04 December 2018

1 Introduction

Higgs boson differential cross section measurements are an important probe of the Standard Model (SM) and provide constraints on effects from physics beyond the SM. As almost model independent measurements, they are well suited to be used for a variety of interpretations (e.g. Ref. [1, 2]).
In this Note, the projections of Higgs boson differential cross-sections measured in the $H \to \gamma\gamma$ and $H \to ZZ^* \to 4\ell$ decay channels, as well as results obtained from combining the two decay channels, are shown for the full expected High-Luminosity LHC (HL-LHC [3]) integrated luminosity. Cross-sections are obtained from measured event yields by subtracting the backgrounds and taking into account detector efficiencies, resolutions, acceptances and branching fractions following the methods used in Ref. [4] for the $H \to \gamma\gamma$ decay channel, Ref. [5] and Ref. [6] for the $H \to ZZ^* \to 4\ell$, and Ref. [7] for their combination. The projections are obtained by scaling the signal and background Asimov datasets used for the Run2 analyses to the HL-LHC expected integrated luminosity of 3 ab^{-1}.
The performance of the future detector will be comparable to or better than the one in Run2. The higher pileup present in the HL-LHC is assumed to be compensated for by new detectors, reconstruction algorithms and analysis strategies to achieve the same performance as in Run2. Two different scenarios in the context of the HL-LHC are studied: in the first, the systematic uncertainties are considered to be the same as the Run2 analyses, while in the second expected improvements in systematic uncertainties are taken into account. In the latter, the current Run2 systematic uncertainties are scaled following Ref. [3].
The observables studied include the Higgs boson transverse momentum p_{T}^{H} and rapidity $|y^{H}|$, the number of jets $\mathrm{N_{jets}}$ with jet transverse momentum above 30 GeV, and the leading jet transverse momentum p_{T}^{j1}. For the $H \to \gamma\gamma$ channel, a different projection was performed in Ref. [8] for the p_{T}^{H} using different pileup and systematic uncertainties scenarios, as well as a different estimation technique in the high p_{T}^{H} regime. For the $H \to ZZ^* \to 4\ell$ channel, projections for the $|y^{H}|$ and p_{T}^{H} were made taking into account improvements in ATLAS Muon Spectrometer [9]. In this note, the p_{T}^{H} distribution is further studied by adding a new higher-p_{T} bin with respect to the previous projections.
The methodology followed for this study is discussed in Section 2. Section 3 presents the results. The conclusions are reported in Section 4.

2 Analysis Strategy

This study aims to provide an estimated precision for the HL-LHC measurements of the $H \to \gamma\gamma$, $H \to ZZ^* \to 4\ell$, and combined differential cross sections for 3 ab^{-1}. The projections are performed using Asimov datasets matching the 2015-2017 luminosity, which are scaled to the expected integrated luminosity of 3 ab^{-1} and center-of-mass energy of $\sqrt{s}$ = 14 TeV [10]. The extrapolations are based on the Run2 analyses using an integrated luminosity of 36 fb^{-1} [4, 5, 7], with the exception of the p_{T}^{H} observable in $H \to ZZ^* \to 4\ell$ where the measurement based on 80 fb^{-1} is used [6]. For the combination, since there are some observables where the binning choice is more granular in one channel than in the other, the bins with higher granularity are summed and combined with the corresponding bin of the other channel. Measurements are based on maximizing the profile-likelihood ratio

$$\Lambda(\vec{\sigma}) = \frac{\mathcal{L}(\vec{\sigma}, \hat{\hat{\theta}}(\vec{\sigma}))}{\mathcal{L}(\hat{\vec{\sigma}}, \hat{\theta})} \tag{1}$$

where $\vec{\sigma}$ is a vector whose elements correspond to the Higgs boson production cross section of each bin for a given observable, θ the nuisance parameters, which correspond to the systematic uncertainties considered,

and $\mathcal{L}$ the likelihood function, which includes the signal extraction, correction to particle level, and extrapolation to the total phase space. The $\hat{\vec{\sigma}}$ and $\hat{\theta}$ terms denote the unconditional maximum-likelihood estimate of the parameters, and $\hat{\hat{\theta}}(\vec{\sigma})$ is the conditional maximum-likelihood estimate for the given parameter values. Under certain assumptions, the effects of foreseen changes to background measurements in each analysis are modeled. Previous measurements in the $H \to ZZ^* \to 4\ell$ channel have taken the normalization of the dominant background, non-resonant SM ZZ^* production, from MC simulation: in the future, this normalization will likely be a parameter of the fit, constrained by the $m_{4\ell}$ sidebands. In the $H \to \gamma\gamma$ channel, the uncertainties on the background parameterization (spurious signal) are largely due to limited statistics in the MC and the data sidebands: for HL-LHC we expect to develop new methods which should render these uncertainties negligible. As with the Run2 results, the combined cross sections, as well as the cross sections in the individual channels, are extracted for the total phase space, and hence are slightly more model-dependent than the cross section measurements in the individual channels performed in Run2, which are extracted in fiducial phase spaces close to the selection criteria for reconstructed events in the detector. The center-of-mass energy increase is taken into account by applying a scale factor to the event yields, neglecting any change in the kinematic distributions, but taking into consideration the different production process composition for each observable bin. Among the four measured observables, the Higgs boson transverse momentum is of particular importance, since it can be used to test perturbative QCD calculations and it is also sensitive to the Lagrangian structure of the Higgs boson interactions [11]; therefore for this study the p_{T}^{H} measurement range was extended up to 1 TeV, with the highest-p_{T}^{H} bin defined to be $p_{\mathrm{T}}^{H} \in [350\ \mathrm{GeV}, 1\ \mathrm{TeV}]$. Such a bin, while already present in the $H \to ZZ^* \to 4\ell$ 80 fb^{-1} analysis, is not included in the $H \to \gamma\gamma$ Run2 measurement, which, as described in Ref. [4], gathered all the events beyond $p_{\mathrm{T}}^{H} = 350$ GeV in an overflow bin. For the projections, to construct a measurement for a bin $p_{\mathrm{T}}^{H} \in [350\ \mathrm{GeV}, 1000\ \mathrm{GeV}]$, the signal and background shapes of the overflow bin have been used, as well as the expected background and signal in this p_{T}^{H} range.

2.1 Systematic uncertainties

Systematic uncertainties are modeled as nuisance parameters in the fit. The impact of some systematic uncertainties is reduced to reflect expected improvements in the years leading up to the HL-LHC (Table 1) [3]. The theoretical and experimental uncertainties related to jet reconstruction and luminosity determination are expected to be ameliorated due to detector upgrades and measurements. The uncertainties related to the photon energy scale and resolution are scaled down, considering that the large amount of data expected and a better knowledge of the detector itself will allow for a more precise energy calibration. The uncertainties related to photon reconstruction, identification, and isolation are also scaled down, assuming that new methods will mitigate the higher pileup environment, which will allow the achievement of a better precision than the current one. Additionally, changes to the background estimation described in the previous section also affect the associated systematic uncertainties. For the $H \to \gamma\gamma$ analysis, the uncertainty related to the background modeling is set to zero regardless of whether the other systematic uncertainties are scaled. In the $H \to ZZ^* \to 4\ell$ channel, the uncertainties on the ZZ irreducible background are scaled such that their sum in quadrature matches the normalization uncertainty expected from the new estimation procedure. Uncertainties affecting the shape of the ZZ background are neglected.

Table 1: A summary list of the systematic uncertainties expected to be improved. The table briefly describes these uncertainties and specifies the amount by which they are scaled.

Systematic Uncertainties	Scale Factor
Jet energy scale, forward region	Set to 0
Jet energy scale, Jet punch-through	Set to 0
High-p_{T} jet energy scale	Set to 0
$H \to \gamma\gamma$ background modeling	Set to 0
4ℓ m_H	Scaled by 0.25
PDF	Scaled by 0.41
Jet flavor	Scaled by 0.5
Jet energy scale	Scaled by 0.5
Pileup modelling	Scaled by 0.5
QCD scale	Scaled by 0.5
Underlying event and parton shower modeling	Scaled by 0.5
Higgs branching ratios	Scaled by 0.5
Photon energy scale and resolution	Scaled by 0.8 [1]
Photon reconstruction, ID, and isolation	Scaled by 0.8
$qq \to ZZ$ irreducible background	Set to 2%
Luminosity	Set to 1% of expected integrated luminosity

3 Results

The results of the HL-LHC projection of the differential cross section measurements are shown in Figure 1, for the $H \to \gamma\gamma$ decay channel, Figure 2, for the $H \to ZZ^* \to 4\ell$ decay channel, and Figure 3, for the combination of the two aforementioned decay channels. The dominant systematic uncertainties for the $\mathrm{N_{jets}}$ and $|y^H|$ measurements are from luminosity and pileup, for p_{T}^{j1} the jet flavour (quark or gluon) composition and the Higgs boson kinematics, and for p_{T}^H the photon identification efficiency and the luminosity. A summary of the expected p_{T}^H bins sensitivity is presented in Table 2 for the three channels. These results show that the highest p_{T}^H bin will be sensitive to the quark top mass effects in the SM loop of the gluon fusion Higgs production according to theoretical predictions [12, 13].

[1] The impact of scaling down the photon energy scale and resolution uncertainty further down from a factor of 0.8 to 0.5 is found to be negligible.

Table 2: Summary of the expected relative uncertainty of the measurements in each p_{T}^{H} bin for the (a) $H \to \gamma\gamma$ decay channel, (b) $H \to ZZ^{*} \to 4\ell$ decay channel, as well as (c) their combination.

Bin [GeV]	Relative uncertainty [%] Without Sys.	Relative uncertainty [%] With Unscaled Syst.	Relative uncertainty [%] With Scaled Syst.
0, 10	4.7	6.5	5.3
10, 20	3.9	5.9	4.6
20, 30	4.3	6.2	4.9
30, 45	4.1	6.0	4.7
45, 60	4.9	6.5	5.4
60, 80	5.0	6.7	5.7
80, 120	4.3	6.0	4.9
120, 200	3.4	5.4	4.2
200, 350	3.9	6.3	5.1
350, 1000	7.4	9.5	8.7

(a)

Bin [GeV]	Relative uncertainty [%] Without Sys.	Relative uncertainty [%] With Unscaled Syst.	Relative uncertainty [%] With Scaled Syst.
0, 10	5.5	9.0	8.3
10, 15	6.1	8.1	7.6
15, 20	6.2	8.9	8.3
20, 30	4.6	6.9	6.3
30, 45	4.3	6.3	5.7
45, 60	5.2	6.8	6.2
60, 80	5.4	6.8	6.3
80, 120	4.9	6.2	5.7
120, 200	5.6	6.7	6.4
200, 350	9.4	13.2	13.1
350, 1000	23	24	23

(b)

Bin [GeV]	Relative uncertainty [%] Without Sys.	Relative uncertainty [%] With Unscaled Syst.	Relative uncertainty [%] With Scaled Syst.
0, 10	3.2	5.5	4.5
10, 20	3.0	4.8	3.8
20, 30	2.8	5.0	3.9
30, 45	2.7	4.7	3.6
45, 60	3.2	5.0	4.1
60, 80	3.3	5.1	4.2
80, 120	2.9	4.6	3.7
120, 200	2.7	4.4	3.5
200, 350	3.4	5.4	4.5
350, 1000	6.8	8.7	8.2

(c)

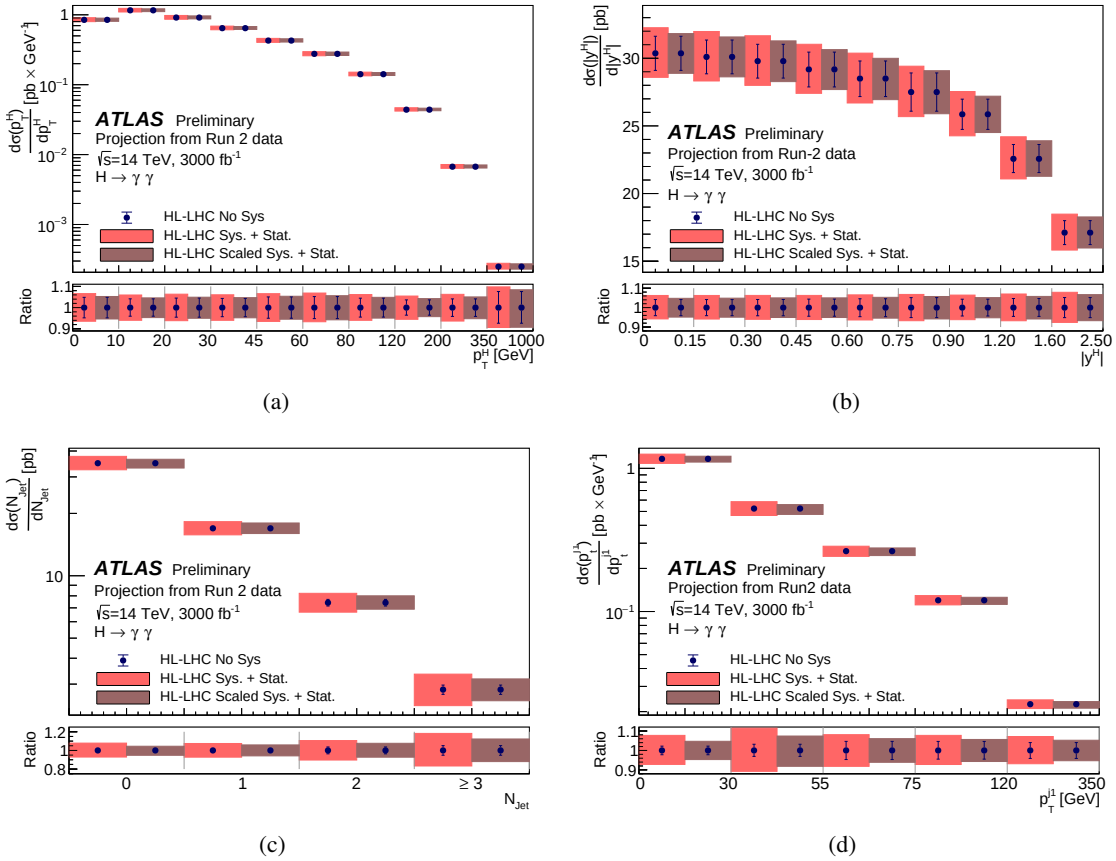

Figure 1: Differential cross section measurements in the total phase space extrapolated to the full HL-LHC luminosity for the $H \rightarrow \gamma\gamma$ decay channel for (a) Higgs boson transverse momentum p_{T}^{H}, (b) Higgs boson rapidity $|y^{H}|$, (c) number of jets $\mathrm{N_{jets}}$ with $p_{\mathrm{T}} > 30$ GeV, and (d) the transverse momentum of the leading jet p_{T}^{j1}. For each point both the statistical (error bar) and total (shaded area) uncertainties are shown. Two scenarios are shown: one with the current Run2 systematic uncertainties and one with scaled systematic uncertainties.

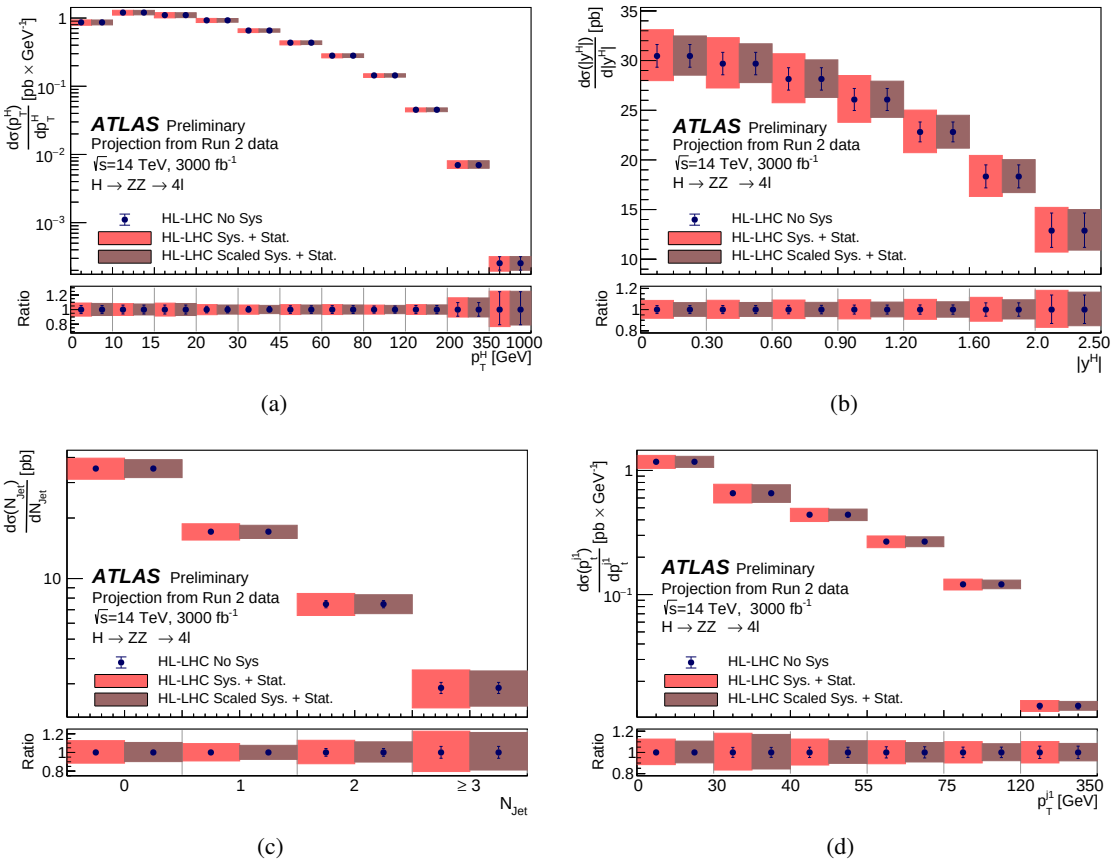

Figure 2: Differential cross section measurements in the total phase space extrapolated to the full HL-LHC luminosity for the $H \rightarrow ZZ^* \rightarrow 4\ell$ decay channel for (a) Higgs boson transverse momentum p_{T}^{H}, (b) Higgs boson rapidity $|y^{H}|$, (c) number of jets $\mathrm{N_{jets}}$ with $p_{\mathrm{T}} > 30$ GeV, and (d) the transverse momentum of the leading jet p_{T}^{j1}. For each point both the statistical (error bar) and total (shaded area) uncertainties are shown. Two scenarios are shown: one with the current Run2 systematic uncertainties and one with scaled systematic uncertainties.

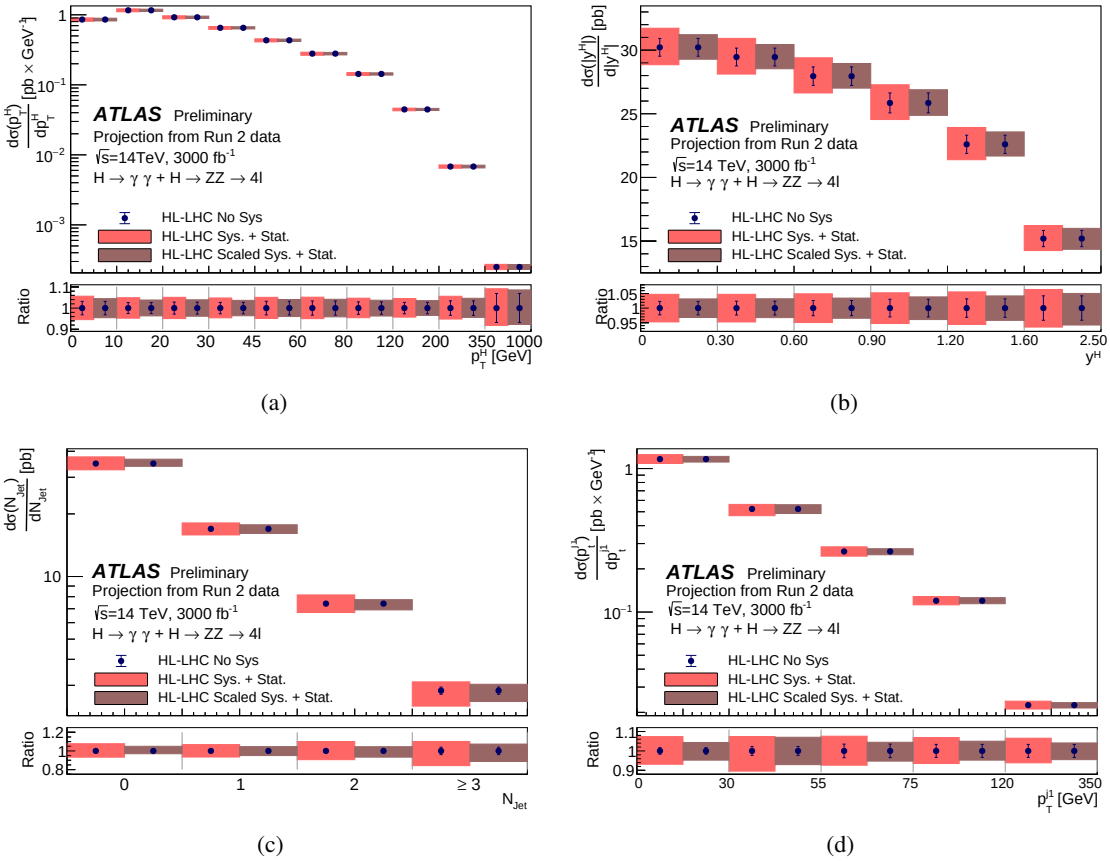

Figure 3: Differential cross sections in the total phase space extrapolated to the full HL-LHC luminosity for the combination of the $H \to \gamma\gamma$ and $H \to ZZ^* \to 4\ell$ decay channels for (a) Higgs boson transverse momentum p_{T}^{H}, (b) Higgs boson rapidity $|y^{H}|$, (c) number of jets $\mathrm{N_{jets}}$ with $p_{\mathrm{T}} > 30$ GeV, and (d) the transverse momentum of the leading jet p_{T}^{j1}. For each point both the statistical (error bar) and total (shaded area) uncertainties are shown. Two scenarios are shown: one with the current Run2 systematic uncertainties and one with scaled systematic uncertainties.

4 Conclusion

Projections for measurements of Higgs boson differential cross sections at the HL-LHC were presented. For a binning similar to what is used in current Run2 measurements, the uncertainties are expected to range between 3% and 20%. Furthermore, the high-p_{T}^{H} bin ($p_{\mathrm{T}}^{H} \in$ [350 GeV, 1 TeV]) will be accessible with a relative precision of about 8% after combining the $H \to \gamma\gamma$ and $H \to ZZ \to 4\ell$ decay channels, and it will be sensitive to the quark top mass effects in the SM loop of the gluon fusion Higgs production according to theoretical predictions [12, 13]. With the increased statistical precision, systematic uncertainties will play an important role for $|y^{H}|$, $\mathrm{N}_{\mathrm{jets}}$, p_{T}^{j1}, and all p_{T}^{H} bins except the one with the highest p_{T}, which will still be statistically limited. Such improved measurements will allow the single and combined measurements to further probe the SM with unprecedented precision and to test for indications of physics beyond the SM.

References

[1] ATLAS Collaboration, *Constraints on non-Standard Model Higgs boson interactions in an effective Lagrangian using differential cross sections measured in the $H \to \gamma\gamma$ decay channel at $\sqrt{s} = 8$ TeV with the ATLAS detector*, Phys. Lett. B **753** (2016) 69, arXiv: 1508.02507 [hep-ex].

[2] ATLAS Collaboration, *Measurement of inclusive and differential cross sections in the $H \to ZZ^* \to 4\ell$ decay channel in pp collisions at $\sqrt{s} = 13$ TeV with the ATLAS detector*, JHEP **10** (2017) 132, arXiv: 1708.02810 [hep-ex].

[3] ATLAS Collaboration, *Expected performance of the ATLAS detector at HL-LHC*, (in progress).

[4] ATLAS Collaboration, *Measurements of Higgs boson properties in the diphoton decay channel with 36 fb^{-1} of pp collision data at $\sqrt{s} = 13$ TeV with the ATLAS detector*, Phys. Rev. D **98** (2018) 052005, arXiv: 1802.04146 [hep-ex].

[5] ATLAS Collaboration, *Measurement of inclusive and differential cross sections in the $H \to ZZ^* \to 4\ell$ decay channel in pp collisions at $\sqrt{s} = 13$ TeV with the ATLAS detector*, JHEP **10** (2017) 132, arXiv: 1708.02810 [hep-ex].

[6] ATLAS Collaboration, *Measurements of the Higgs boson production, fiducial and differential cross sections in the 4ℓ decay channel at $\sqrt{s} = 13$ TeV with the ATLAS detector*, (2018), URL: https://cds.cern.ch/record/2621479.

[7] ATLAS Collaboration, *Combined measurement of differential and total cross sections in the $H \to \gamma\gamma$ and the $H \to ZZ^* \to 4\ell$ decay channels at $\sqrt{s} = 13$ TeV with the ATLAS detector*, (2018), arXiv: 1805.10197 [hep-ex].

[8] ATLAS Collaboration, *Technical Design Report for the Phase-II Upgrade of the ATLAS LAr Calorimeter*, (2017), URL: https://cds.cern.ch/record/2285582.

[9] ATLAS Collaboration, *Technical Design Report for the Phase-II Upgrade of the ATLAS Muon Spectrometer*, (2017), URL: https://cds.cern.ch/record/2285580.

[10] D. de Florian et al., *Handbook of LHC Higgs Cross Sections: 4. Deciphering the Nature of the Higgs Sector*, (2016), arXiv: 1610.07922 [hep-ph].

[11] M. Grazzini, A. Ilnicka, M. Spira and M. Wiesemann, *Modeling BSM effects on the Higgs transverse-momentum spectrum in an EFT approach*, JHEP **03** (2017) 115, arXiv: 1612.00283 [hep-ph].

[12] J. M. Lindert, K. Kudashkin, K. Melnikov and C. Wever, *Higgs bosons with large transverse momentum at the LHC*, Phys. Lett. **B782** (2018) 210, arXiv: 1801.08226 [hep-ph].

[13] S. P. Jones, M. Kerner and G. Luisoni, *Next-to-Leading-Order QCD Corrections to Higgs Boson Plus Jet Production with Full Top-Quark Mass Dependence*, Phys. Rev. Lett. **120** (2018) 162001, arXiv: 1802.00349 [hep-ph].